NANO LETTERS

Letter

pubs.acs.org/NanoLett

Synthesis of Lateral Heterostructures of Semiconducting Atomic Layers

Xin-Quan Zhang,† Chin-Hao Lin,† Yu-Wen Tseng, Kuan-Hua Huang, and Yi-Hsien Lee*

Materials Science and Engineering, National Tsing-Hua University, Hsinchu 20013, Taiwan

Supporting Information

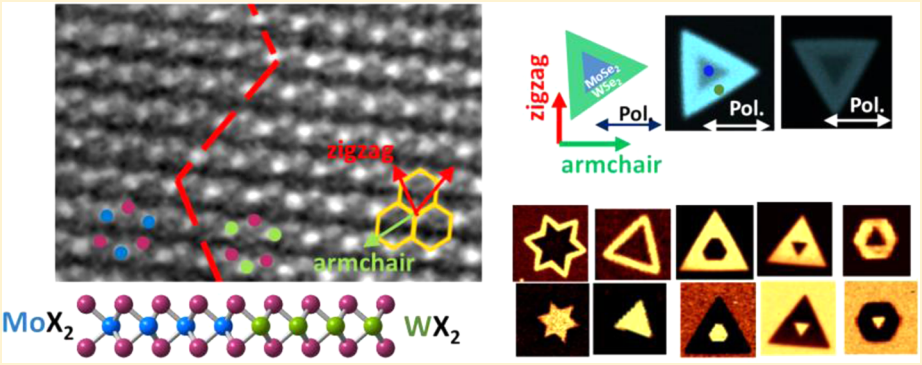

ABSTRACT: Atomically thin heterostructures of transition-metal dichalcogenides (TMDs) with various geometrical and energy band alignments are the key materials for next generation flexible nanoelectronics. The individual TMD monolayers can be adjoined laterally to construct in-plane heterostructures, which are difficult to reach with the laborious pick-up-and-transfer method of the exfoliated flakes. The ability to produce copious amounts of high quality layered heterostructures on diverse surfaces is highly desirable but it has remained a challenging issue. Here, we have achieved a direct synthesis of lateral heterostructures of monolayer TMDs: MoS_2–WS_2 and $MoSe_2$–WSe_2. The synthesis was performed using ambient-pressure chemical vapor deposition (CVD) with aromatic molecules as seeding promoters. We discuss possible growth behaviors, and we examine the symmetry and the interface of these heterostructures using second-harmonic generation and atomic-resolution scanning TEM. We found that the one-dimensinal (1D) interface of the lateral heterostructures picks the zigzag direction of the lattice instead of the armchair direction. Our method offers a controllable synthesis to obtain high-quality in-plane heterostructures of TMD atomic layers with 1D interface geometry.

KEYWORDS: *heterostructure, transition metal dichalcogenides, 2d materials, monolayer, CVD*

The heterostructure of materials with various geometrical and energy band alignments can exhibit electronic properties macroscopically different from their constituent materials.[1−13] They offer novel phenomena in semiconducting multiple quantum wells, such as interlayer Coulomb drag between charge carriers and phonons, exciton Bose condensation, emergent massive Dirac Fermions and fractal quantum Hall, and diverse applications including the quantum cascade laser and the high-mobility two-dimensional electron gas.[1,7−10] More recently, the ability to construct atomically thin heterostructures has allowed for the first realization of the Hofstadter butterfly in vertically stacked graphene/h-BN heterostructures[7−9] and interlayer excitons in transition metal dichalcogenides (TMD) heterojunctions.[15−18] These monolayer materials are the building blocks for constructing various heterostructures with atomically sharp interfaces in the absence of dangling bonds.[3,19−28] Moreover, the heterostructures can be functionalized by energy band alignments and also by electrostatic gating to control the charge doping concentration.[26,29,30] In particular, the diverse properties of individual TMDs monolayer (such as MoS_2, $MoSe_2$, WS_2, and WSe_2) provide promising candidates to further construction of various heterostructures for nanoscience and next generation optoelectronic and valleytronic devices.[4,22,31−37]

The band structures and diverse performances of these heterostructures are significantly determined by their crystalline phases and symmetry, and interface quality.[38,39] Second harmonic generation (SHG) was considered as a robust characterization tool on interfaces, symmetry, and twisting angles of the atomic layers in the heterostructures.[39−47] The analytic spherical aberration corrected scanning transmission electron microscopy (Cs-corrected STEM) is promising for the characterization of crystal structures and the interfaces on the nanoscale through its subatomic resolution and capabilities in the chemical mappings of light elements.[48−50] Recently, some unique performances, enhanced electric performances with

Received: September 29, 2014
Revised: November 20, 2014
Published: December 11, 2014

edge-contact geometry, were discovered with the one-dimensional (1D) contact of graphene and the 1D interface in the lateral heterojunctions of diverse atomic layers.[11−14,51,71,72] Geometrical alignments of the atomic layers, including their interface geometry and stacking sequences, may realize the construction of various heterostructures with various interface geometries, band structures, and symmetry. However, most studies on heterostructures to date have been commonly achieved by pick up-and-transfer processes with exfoliated flakes or CVD monolayers.[26,39,51] Direct control of the heterojunctions with atomically sharp interfaces in the heterostructure is highly demanded. Hence, a direct feasible synthetic process to realize in-plane heteroepitaxial growth of the atomic layers on diverse monolayer surfaces with different 1D interface is essential. Chemical vapor deposition is promising for scalable synthesis of high-quality atomic layers of diverse van der Waals (vdw) materials.[52−61] In this work, we realized the synthesis of lateral heterostructures by the direct growth of semiconducting TMD atomic layers on diverse monolayer surfaces using ambient pressure chemical vapor deposition (APCVD) with aromatic molecules as seeding promoters. Different 1D interface of TMD monolayers was achieved in the lateral heterostructures of MoS_2−WS_2 and $MoSe_2$−WSe_2 atomic layers. The symmetry and interfaces of the heterojunctions and interfaces were further investigated with Cs-corrected STEM and SHG imaging.

The schematic illustration of the experimental setup and detailed parameters of the synthesis of TMD atomic layers and their heterostructures are shown in Figure 1a and Supporting Information S1. The synthesis is achieved using APCVD with perylene-3,4,9,10-tetracarboxylic acid tetrapotassium salt (PTAS) as seeding promoters. More details on substrates treatments and preparation of the seeding promoters were presented in previous papers and Supporting Information S2.[62,63] A one-inch diameter furnace and a homemade quartz reactor were designed for the precise control of the gas flow and reactions of the starting reactants. For a high evaporation temperature of WO_3, the WO_3 powders were filled in the homemade quartz reactor with a transfer tube in tunable length to enable a stable vapor flow of the WO_{3-x} that is reactant evaporated from the high temperature zone to react with S or Se on substrate surfaces at each specific temperature and distance. In the low temperature zone, individual TMD monolayers could be successfully synthesized with a temperature range from 650 to 750 °C. The growth of Mo-based TMD atomic layer is much easier than that of W-based TMD ones because MoO_3 vapor pressure is much higher than WO_3 one at specific growth temperature. By carefully controlling the amount of reactants, we can achieve lateral heterostructures of different TMD atomic layers. Figure 1 presents characterizations and comparisons of the diverse lateral heterostructure of TMD atomic layers with 1D interface. Figure 1b illustrates typical configuration of lateral heterostructure of single layer TMD atomic layers; single layers of WS_2 (WSe_2) was found to joint laterally to the MoS_2 ($MoSe_2$) edges and to maintain its triangular domain shape with atomically sharp 1D heterointerfaces. The growth of W-based atomic layers was initiated from the edges of as-grown Mo-based monolayers and they follow the domain shape for their following lateral growth. Furthermore, large area in-plane heterostructure is possible to reach with a longer growth time and a low growth temperature of 650−700 °C, as shown in Supporting Information S4. A typical island growth mode appears in a reduced growth

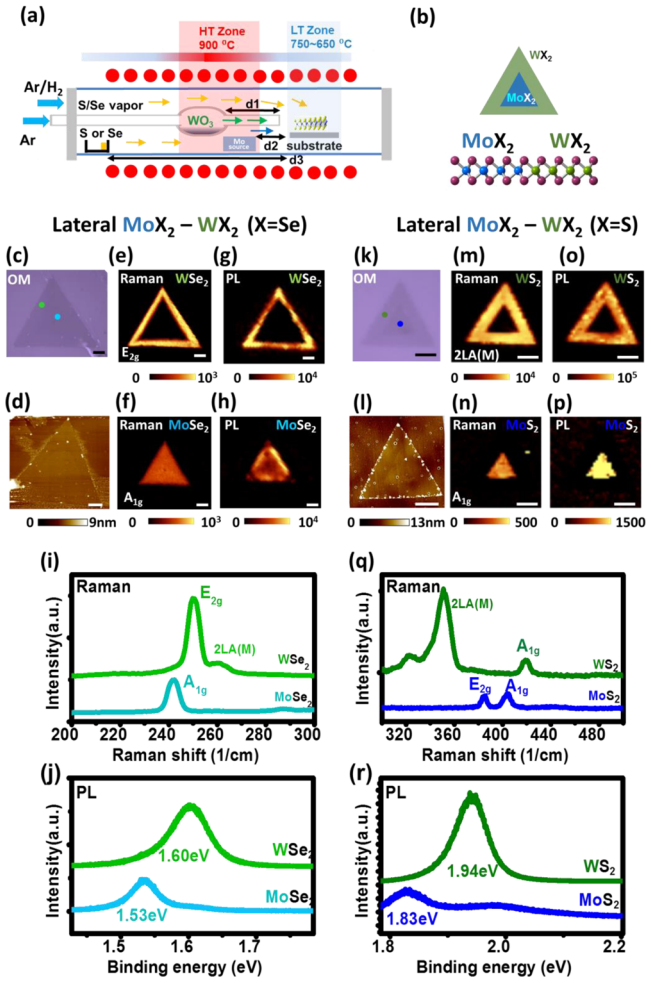

Figure 1. Synthesis of lateral heterostructures of TMD atomic layers with 1D interface. Schematic illustration of (a) experimental APCVD setup and (b) the lateral heterostructure of TMD atomic layers. Characterizations of lateral heterostructure of $MoSe_2$−WSe_2 monolayers: : (c) optical microscopy (OM) and (d) atomic force microscopy (AFM) images; Raman mapping of (e) WSe_2, E_{2g} mode, and (f) $MoSe_2$, A_{1g} mode; PL mapping of (g) WSe_2 and (h) $MoSe_2$; (i) Raman spectrum; and (j) PL spectrum of WSe_2 and $MoSe_2$ area in the heterostructure as marked in panel c. Characterizations of lateral heterostructure of MoS_2−WS_2 monolayers: (k) OM and (l) AFM images; Raman mapping of (m) WS_2, 2LA(M) mode, and (n) MoS_2 - A_{1g} mode; PL mapping of (o) WS_2 and (p) MoS_2; (q) Raman spectrum; and (r) PL spectrum of WS_2 and MoS_2 area in the heterostructure as marked in panel k. (Scale bar: 5 μm).

temperature range lower than 600 °C. The growth behavior and uniformity of the growth of the TMD atomic layers are sensitive to growth temperature, reactant flux, gas flow, and the concentration of seeding promoters. Three typical Mo sources for the synthesis, including MoO_3 powders, thermal evaporated MoO_{3-x} thin layers on Si, and stoichiometric MoX_2 (X = S, Se) powders, were carefully studied and compared for better understanding of the growth behavior, as shown in Supporting Information S4. With the oxide powders as starting materials, the growth always display a simple growth of MoS_2 ($MoSe_2$) monolayers under S (Se) vapor due to a high vapor pressure of the molybdenum oxide powders (MoO_{3-x}). In contrast, TMD atomic layers were able to grow laterally on other monolayer edges using stoichiometric MoS_2 ($MoSe_2$) powders or a small piece of Si covered with thermal evaporated 10 nm MoO_{3-x}

dx.doi.org/10.1021/nl503744f | Nano Lett. 2015, 15, 410−415

thin layer. The growth might result from a reduced vapor flow of the Mo reactants because the entire process involves the decomposition of the thin layer or of stoichiometric powders in high temperature and their transport from the high temperature zone to the low temperature zone for further growth. The heterostructure based on pure TMD atomic layers requires a pure vapor of S (Se) to avoid alloying of the TMD atomic layers in a mixed S and Se vapor.[64−66] Note that vertical heterostructures can be obtained using our growth method. The growth behavior as well as the possibility of alloying in such heterostructures requires careful investigation in future works. In this study, the lateral heterostructure of pure TMD monolayers is mainly observed for a low temperature CVD growth using aromatic molecules as seeding promoters.

To study the spectroscopy and photoluminescence (PL) performance of the as-grown lateral heterostructure, the Raman and PL spectra of various TMD atomic layers in the lateral heterostructure were taken at the location shown in Figure 1c (WSe_2−$MoSe_2$) and Figure 1k (WS_2−MoS_2), respectively. In Figure 1i and j, the E_{2g} and A_{1g} modes of Raman band of single-layer WSe_2 are located at 249.9 and 259.9 cm^{-1}, whereas those of the $MoSe_2$ are at 286.7 and 241.6 cm^{-1}. In contrast, the E_{2g} and A_{1g} modes of single-layer WS_2 are located at 349.4 and 418.4 cm^{-1}, whereas those of the monolayer MoS_2 are at 384.4 and 402.4 cm^{-1}, and those values are similar to that of the individual TMD monolayer reported elsewhere.[59,67−70] The PL peaks of the $MoSe_2$ and the WSe_2 in the lateral heterostructure are located approximately at 810 and 770 nm, whereas that of the as-grown individual $MoSe_2$ and WSe_2 monolayers are located at 805 and 768 nm, respectively. Raman mapping in a confocal measurement for the lateral heterostructure of TMD atomic layers are shown in Figure 1e−h (WSe_2−$MoSe_2$) and Figure 1m−p (WS_2−MoS_2), respectively. A clear contrast among diverse TMD atomic layers is observed in the Raman mapping images, demonstrating an in-plane heterojunction signature of the TMD atomic layers. Note that the Raman and PL intensity of the TMD monolayers in the lateral heterostructure is uniform and intense, indicating a good crystallinity and a low defects concentration of the as-grown lateral heterostructure. Other than the common triangular shape of the lateral heterostructure, a star-like shape was sometimes observed in the lateral heterostructure of WSe_2−$MoSe_2$ with an increased thickness, which might be correlated to defects in the growth and fundamental processes of nucleation and growth. More detailed information on thickness identification and domain shapes of the lateral heterostructures are shown in Supporting Information S5.

The atomic and chemical configurations of individual TMD monolayers, including MX_2 (M = Mo, W; X = S, Se), and their 1D heterointerfaces were carefully identified using a Cs-corrected STEM high-angle annular dark-field (HAADF). The contrast of the STEM-HAADF imaging, so-called *Z*-contrast, is proportional to the atomic numbers of the individual M and X atomic column by the angular dark field (ADF) method. Figure 2a−e demonstrates the honeycomb structure of MX_2 and the microstructure of lateral 1D heterointerface. At the white arrow marked in Figure 2a, the heteroepitaxial growth can be initiated and the atomic layer could grow laterally on the "1D interfaces" of the TMD monolayer. A uniform lateral growth along the MoS_2 domain edges illustrates that the lateral growth would follow the domain shape of the monolayer and would maintain a single crystalline signature of the in-plane heterostructure. The lateral heteroepitaxial growth only appears in the atomic

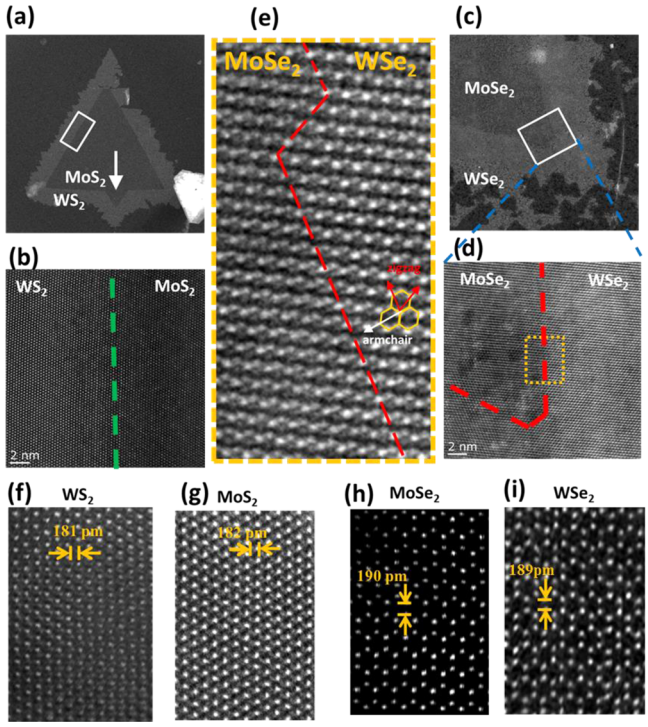

Figure 2. Atomic-resolution imaging of lateral heterojunctions and individual TMD monolayers with Cs-corrected STEM-HAADF. (a, c) Low magnification images and (b, d) high resolution HAADF images of the WS_2−MoS_2 and the WSe_2−$MoSe_2$ lateral heterostructures, respectively. High resolution STEM HAADF image of (e) hetero-interface of the WSe_2−$MoSe_2$ lateral heterostructure. (f−i) individual TMD-MX2 (M = Mo, W; X = S, Se) atomic layers.

layer of vdw materials and shows a clear contrast to conventional epitaxial growth, which has potential for further studies of in-plane hybrid heterostructures. Atomic resolution imaging of the 1D heterointerfaces of WS_2−MoS_2 and WSe_2−$MoSe_2$ lateral heterostructures are demonstrated in Figure 2b and Figure 2d−e, respectively. A schematic illustration of the zigzag and the armchair direction in honeycomb lattice is labeled in Figure 2e, and the 1D heterointerfaces prefer to be aligned in the zigzag direction. In Figure 2f−i, the honeycomb M−X spacing of sulfides is about 181−182 pm, whereas that of selenides is about 189−190 pm. The filtered images provide convincing evidence that the M−X spacing can be clearly resolved by Cs-STEM technology. The contrast between M and X element would significantly depend on the atomic number (*Z*) difference of the atomic column, so image contrast of the selenides should be better than that of the sulfides. Based on the identification of SAED and high-resolution image, the space group of the specimens was *P*63/*mmc* among the various MX_2 samples. The contrast and spacing of dumbbell depended on the materials of monolayers. The HAADF image intensities were directly proportional to about $Z^{1.7}$.[48] We supposed that the intensity variation among diverse MX_2 samples might be due to the difference of *Z*. Therefore, the HAADF image contrast of the sulfides was too high for a large variation of *Z* so that the sulfur column was difficult to be visualized. These results are in good agreement with atomic models simulated under identical conditions.

Strong second harmonic generation (SHG) signals were observed in TMD layers with an odd layer numbers for the lack of inversion symmetry[39−43] and a nonvanishing second-order

dx.doi.org/10.1021/nl503744f | *Nano Lett.* 2015, 15, 410−415

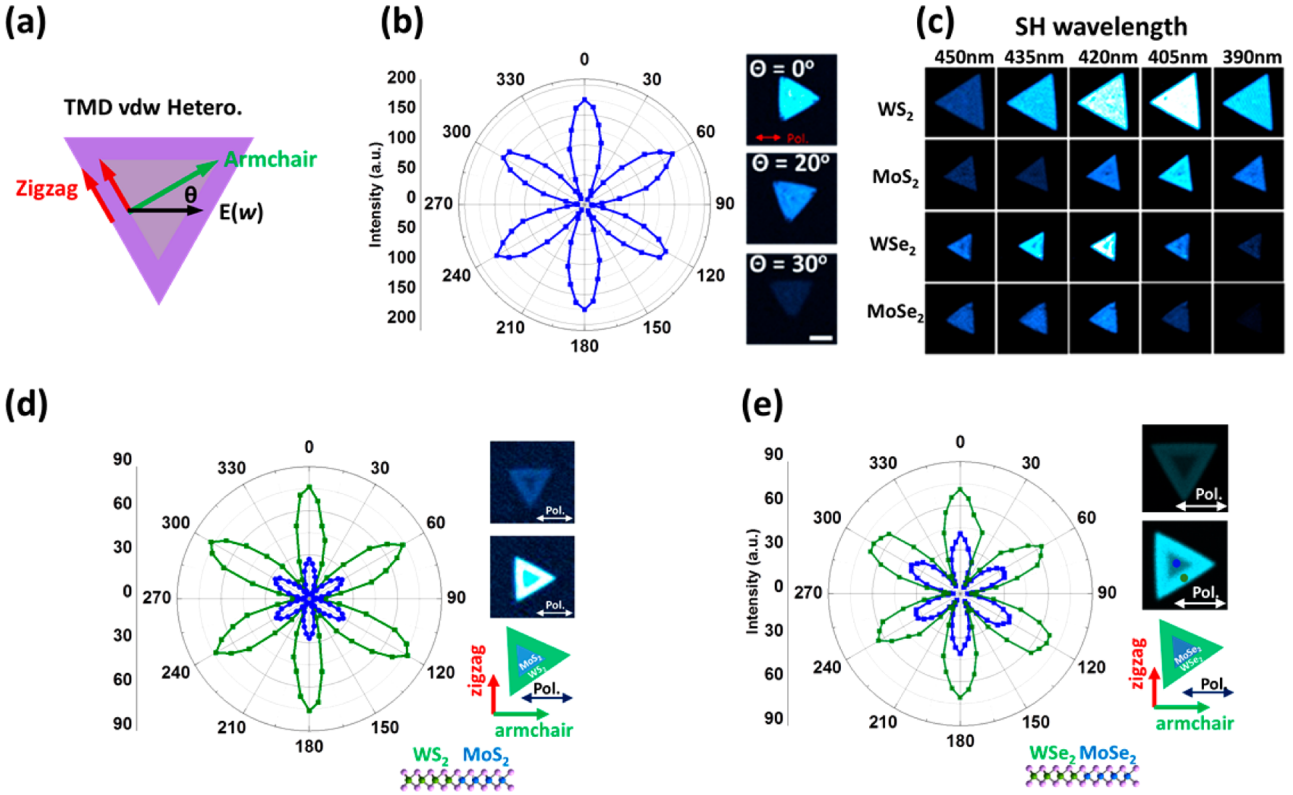

Figure 3. Identification of symmetry and edge structures of lateral TMD heterostructures with second harmonic generation (SHG) analysis. (a) Schematic illustration of orientation dependence among laser polarization and the two typical edges in individual TMD flake or lateral heterostructures of TMD atomic layers. (b) Polar plot of the parallel polarization SH intensity. The blue dots are the experiment data and solid line is fitting curve. Angular dependent SHG imaging of WS_2 flake under a parallel laser polarization. Scalar bar: 10 μm (c) Wavelength dependence of SHG images of diverse CVD-TMD single crystal flakes: MX_2 (M = Mo, S; X = S, Se). (d) Polar plot of the parallel polarization SH intensity of lateral heterostructure of WS_2−MoS_2 atomic layers. (e) Polar plot of the parallel polarization SH intensity of lateral heterostructure of WSe_2−$MoSe_2$ atomic layers. SHG intensity of WS_2 (WSe_2) and MoS_2 ($MoSe_2$), represented in green and blue dots, are measured on the periphery and center area of the heterostructure flake, respectively. Minimum and maximum SHG images of the lateral heterostructures were obtained at $\theta = 30°$ and $\theta = 0°$.

susceptibility.[44] In contrast, TMD samples with an even layer number may hold inversion symmetry and show a reduced SHG signal. However, it is possible to realize a broken symmetry in bilayer TMD by interlayer rotation.[43,46] Structural symmetry of the TMD layers can be determined by analyzing the SHG polarization.[45] As shown in Figure 3a, the intensity of parallel polarization components of SHG can be described as $I_{\parallel} = I_0 \cos^2(3\theta)$, where I_0 is the maximum SHG intensity and θ is the angle between the polarization of incident beam and the armchair direction.[39−42,46] Figure 3b shows a polar plot of SHG intensity from a WS_2 flake. A clear 6-fold symmetry was observed. The experimental data were obtained from the average pixel intensity of the WS_2 SHG image over a range of angles within a 180° rotation of the sample and the data were fitted by $\cos^2\theta$ function. Figure 3b also presents angular dependent SHG imaging of a WS_2 flake. The polarization of the incident laser beam was labeled with an arrow. By rotating the sample, the parallel polarization component of the SH response was enhanced and a maximum intensity SH image is obtained when the bisector of the triangle (armchair direction) is parallel to the incident polarization, indicating that the edge of the triangular TMD flake is in a zigzag configuration. Furthermore, we performed wavelength dependent SHG studies from different TMD flakes on the same substrate. The SHG intensity depends on the local dielectric environment, incident electric field and the second-order nonlinear susceptibility. As shown in Figure 3c, WS_2 and MoS_2 exhibit the maximum SH response as the wavelength of the SH approaches 405 nm. This efficient SH response can be attributed to the enhanced susceptibility due to the increased density of electronic states at the Γ point.[40] On the other hand, the maximum SH response of WSe_2 and $MoSe_2$ occurs as a SH wavelength close to 420 nm. The different SH efficiencies among these TMD flakes is thus a consequence of their different band structures at the Γ point. Figure 3d and e presents a parallel polarization SHG image of the lateral heterostructure of WSe_2−$MoSe_2$ and WS_2−MoS_2, respectively. A clear coherent and 6-fold symmetry is observed on the polar plot of the SHG intensity at the center and on the periphery area of the lateral heterostructures, suggesting that two different TMD atomic layers were crystallized in the same crystalline orientation. Moreover, no suppressed SH was observed along the interface of the lateral TMD heterostructured flakes, which demonstrates a single crystal signature in the in-lateral heterostructure of TMD atomic layers. The maximum SHG image of the lateral WS_2−MoS_2 heterostructure on this TMD flake was obtained at $\theta = 0°$ (the armchair direction parallel to the incident polarization). It is suggested that the heterointerface between two TMD atomic layers is identified to be in zigzag configuration, which is consistent with our TEM observation.

We believe that more interesting physics and deep insights will be wildly explored in the in-plane lateral heterostructures because of a single crystalline signature of the TMD atomic layers and a unique 1D heterointerface. Various interface

dx.doi.org/10.1021/nl503744f | Nano Lett. 2015, 15, 410−415

geometries and heterojunctions of the heterostructures are controllable with the directly epitaxial growth of the TMD atomic layers on various surfaces. This opens a new avenue toward low-dimensional channels and artificial heterostructures using controllable interfaces and junctions of diverse TMD atomic layers.

■ ASSOCIATED CONTENT

Supporting Information

Experimental setup and detailed parameters for the synthesis, preparation of samples and aromatic seeding promoters, scalable synthesis of in-plane heterostructure of monolayer WS_2-MoS_2, influence of starting materials on the CVD growth of the S- and Se-based heterostructure, lateral heterostructure with 1D heterointerface, characterizations (Cs-corrected STEM-HAADF and polarization-resolved second harmonic generation (SHG)), Raman vibration mode frequencies of the lateral heterostructures. Additional figures and tables. This material is available free of charge via the Internet at http://pubs.acs.org.

■ AUTHOR INFORMATION

Corresponding Author

*E-mail: yhlee.mse@mx.nthu.edu.tw. Phone and Fax: +886-3-5715131, ext 33880. Web: www.mse.nthu.edu.tw/~yhlee/.

Author Contributions

†These authors contribute equally. X.Z., Y.T., and K.H. carried out the synthesis. X.Z. and C.L. carried out TEM, Raman, PL and AFM. C.L. performed SHG measurements. Y.H.L. conceived the project and wrote the paper. All authors discussed the results.

Notes

The authors declare no competing financial interest.

■ ACKNOWLEDGMENTS

This research was supported by the National Science Council of the Republic of China (NSC103-2112-M-007-001-MY3 and NSC102-2633-M-007-002 at National Tsing-Hua University). We thank C. S. Chang, P. Y. Lin, M. T. Chang, S. C. Luo, and Prof. L. J. Chen for their technical assistance, and also E. J. Sie, and Prof. M. Dresselhaus (MIT) for fruitful discussions.

■ REFERENCES

(1) Faist, J.; Capasso, F.; Sivco, D. L.; Sirtori, C.; Hutchinson, A. L.; Cho, A. Y. *Science* **1994**, *264*, 553−556.
(2) Alferov, Z. I. *Rev. Mod. Phys.* **2001**, *73*, 767−782.
(3) Geim, A. K.; Grigorieva, I. V. *Nature* **2013**, *499*, 419−425.
(4) Britnell, L.; Ribeiro, R. M.; Eckmann, A.; Jalil, R.; Belle, B. D.; Mishchenko, A.; Kim, Y. J.; Gorbachev, R. V.; Georgiou, T.; Morozov, S. V.; et al. *Science* **2013**, *340*, 1311−1314.
(5) Terrones, H.; Lopez-Urias, F.; Terrones, M. *Sci. Rep.* **2013**, *3*, 1549.
(6) Komsa, H. P.; Krasheninnikov, A. V. *Phys. Rev.* **2013**, *88*, 085318.
(7) Ponomarenko, L. A.; Gorbachev, R. V.; Yu, G. L.; Elias, D. C.; Jalil, R.; Patel, A. A.; Mishchenko, A.; Mayorov, A. S.; Woods, C. R.; Wallbank, J. R.; et al. *Nature* **2013**, *497*, 594−597.
(8) Dean, C. R.; Wang, L.; Maher, P.; Forsythe, C.; Ghahari, F.; Gao, Y.; Katoch, J.; Ishigami, M.; Moon, P.; Koshino.; et al. *Nature* **2013**, *497*, 598−602.
(9) Hunt, B.; Sanchez-Yamagishi, J. D.; Young, A. F.; Yankowitz, M.; LeRoy, B. J.; Watanabe, K.; Taniguchi, T.; Moon, P.; Koshino, M.; Jarillo-Herrero, P.; et al. *Science* **2013**, *340*, 1427−1430.
(10) Gorbachev, R. V.; Geim, A. K.; Katsnelson, M. I.; Novoselov, K. S.; Tudorovskiy, T.; Grigorieva, I. V.; MacDonald, A. H.; Morozov, S. V.; Watanabe, K.; Taniguchi, T.; et al. *Nat. Phys.* **2012**, *8*, 896−901.
(11) Levendorf, M. P.; Kim, C. J.; Brown, L.; Huang, P. Y.; Havener, R. W.; Muller, D. A.; Park, J. *Nature* **2012**, *488*, 627−632.
(12) Liu, Z.; Ma, L. L.; Shi, G.; Zhou, W.; Gong, Y. J.; Lei, S. D.; Yang, X. B.; Zhang, J. N.; Yu, J. J.; Hackenberg, K. P.; et al. *Nat. Nanotechnol.* **2013**, *8*, 119−124.
(13) Liu, L.; Park, J.; Siegel, D. A.; McCarty, K. F.; Clark, K. W.; Deng, W.; Basile, L.; Idrobo, J. C.; Li, A. P.; Gu, G. *Science* **2014**, *343*, 163−167.
(14) Huang, C.; Wu, S.; Sanchez, A.; Peters, J.; Beanland, R.; Ross, J.; Rivera, P.; Yao, W.; Cobden, D.; Xu, X. *Nat. Mater.* **2014**, *13*, 1096−1101.
(15) Rivera, P.; Schaibley, J. R.; Jones A. M. Ross, J. S.; Wu, S.; Aivazian, G.; Klement, P.; Ghimire, N. J.; Yan, J.; Mandrus, D. G.; Wang Yao.; Xiaodong Xu. 2014, *arXiv:1403.4985*. arXiv.org e-Print archive. http://arxiv.org/abs/1403.4985 (accessed Sept 2014).
(16) Lui, J.; Ye, Z.; Ji, C.; Chiu, K. C.; Chou, C. T.; Andersen, T. I.; Means-Shively, C.; Anderson, H.; Wu, J. M.; Kidd, T.; Lee, Y.-H.; He R. 2014, *arXiv:1410.4224*. arXiv.org e-Print archive. http://arxiv.org/abs/1410.4224 (accessed Sept 2014).
(17) Tongay, S.; Fan, W.; Kang, J.; Park, J.; Koldemir, U.; Suh, J.; Narang, D. S.; Liu, K.; Ji, J.; Li, J.; Sinclair, R.; Wu, J. *Nano Lett.* **2014**, *14*, 3185−3190.
(18) Yu, Y.; Hu, S.; Su, L.; Huang, L.; Liu, Y.; Jin, Z.; Purezky, A. A.; Geohegan, D. B.; Kim, K. W.; Zhang, Y.; Cao, L. 2014, *arXiv:1403.6181*. arXiv.org e-Print archive. http://arxiv.org/abs/1403.6181 (accessed Sept 2014).
(19) Sie, E. J.; Lee, Y. -H; Frenzel, A. J.;Kong, J.; Gedik N. 2013, *arXiv:1312.2918*. arXiv.org e-Print archive. http://arxiv.org/abs/1312.2918 (accessed Sept 2014).
(20) Geim, A. K.; Novoselov, K. S. *Nat. Mater.* **2007**, *6*, 183−191.
(21) Watanabe, K.; Taniguchi, T.; Kanda, H. *Nat. Mater.* **2004**, *3*, 404−409.
(22) Wang, Q. H.; Kalantar-Zadeh, K.; Kis, A.; Coleman, J. N.; Strano, M. S. *Nat. Mater.* **2012**, *7*, 699−712.
(23) Wang, H.; Yu, L. L.; Lee, Y. H.; Shi, Y. M.; Hsu, A.; Chin, M. L.; Li, L. J.; Dubey, M.; Kong, J.; Palacios, T. *Nano Lett.* **2012**, *12*, 4674−4680.
(24) Zhu, W.; Low, T.; Lee, Y. H.; Wang, H.; Farmer, D. B.; Kong, J.; Xia, F.; Avouris, P. *Nat. Commun.* **2014**, *5*, 3087.
(25) Yu, W. J.; Liu, Y.; Zhou, H. L.; Yin, A. X.; Li, Z.; Huang, Y.; Duan, X. F. *Nat. Nanotechnol.* **2013**, *8*, 952−958.
(26) Lee, C.-H.; Lee, G.-H.; van der Zande, A. M.; Chen, W.; Li, Y.; Han, M.; Cui, X.; Arefe, G.; Nuckolls, C.; Heinz, T. F.; Guo, J.; et al. *Nat. Nanotechnol.* **2014**, *9*, 676−681.
(27) Carraro, C.; Nemsak, S.; Ozdol, B.; Kang, J. S.; Bechtel, H. A.; Desai, S. B.; Kronast, F.; Unal, A. A.; Conti, G.; Conlon, C.; et al. *Proc. Natl. Acad. Sci. U.S.A.* **2014**, *111*, 6198−6202.
(28) Cheng, R.; Li, D.; Zhou, H.; Wang, C.; Yin, A.; Jiang, S.; Liu, Y.; Chen, Y.; Huang, Y.; Duan, X. 2014, *arXiv:1403.3447*. arXiv.org e-Print archive. http://arxiv.org/abs/1403.3447 (accessed Sept 2014).
(29) Yu, L.; Lee, Y.-H.; Ling, X.; Santos, E. J. G.; Shin, Y. C.; Lin, Y.; Dubey, M.; Kaxiras, E.; Kong, J.; Wang, H.; Palacios, T. *Nano Lett.* **2014**, *14*, 3055−3063.
(30) Furchi, M. M.; Pospischil, A.; Libisch, F.; Burgdörfer, J.; Mueller, T. 2014, *arXiv:1403.2652*. arXiv.org e-Print archive. http://arxiv.org/abs/1403.2652 (accessed Sept 2014).
(31) Liu, X.; Galfsky, T.; Sun, Z., Xia, F.; Lin, E. C.; Lee, Y. H.; Kéna-Cohen S., Menon, V. M. 2014, *arXiv:1406.4826*. arXiv.org e-Print archive. http://arxiv.org/abs/1406.4826 (accessed Sept 2014).
(32) Zaumseil, J. *Science* **2014**, *344*, 702−703.
(33) Zhang, Y. J.; Oka, T.; Suzuki, R.; Ye, J. T.; Iwasa, Y. *Science* **2014**, *344*, 725−728.
(34) Xiao, D.; Liu, G. B.; Feng, W. X.; Xu, X. D.; Yao, W. *Phys. Rev. Lett.* **2012**, *108*, 196802.
(35) Zeng, H. L.; Dai, J. F.; Yao, W.; Xiao, D.; Cui, X. D. *Nat. Nanotechnol.* **2012**, *7*, 490−493.

(36) Mak, K. F.; He, K. L.; Shan, J.; Heinz, T. F. *Nat. Nanotechnol.* **2012**, *7*, 494−498.
(37) Cao, T.; Wang, G.; Han, W.; Ye, H.; Zhu, C.; Shi, J.; Niu, Q.; Tan, P.; Wang, E.; et al. *Nat. Commun.* **2012**, *3*, 887.
(38) Suzuki, R.; Sakano, M.; Zhang, Y. J.; Akashi, R.; Morikawa, D.; Harasawa, A.; Yaji, K.; Kuroda, K.; Miyamoto, K.; Okuda, T.; et al. *Nat. Nanotechnol.* **2014**, *9*, 611−617.
(39) van der Zande, A. M.; Kunstrnann, J.; Chernikov, A.; Chenet, D. A.; You, Y.; Zhang, X.; Huang, P. Y.; Berkelbach, T. C.; Wang, L.; Zhang, F.; et al. *Nano Lett.* **2014**, *14*, 3869−3875.
(40) Kumar, N.; Najmaei, S.; Cui, Q. N.; Ceballos, F.; Ajayan, P. M.; Lou, J.; Zhao, H. *Phys. Rev. B* **2013**, *87*, 161403.
(41) Malard, L. M.; Alencar, T. V.; Barboza, A. P. M.; Mak, K. F.; de Paula, A. M. *Phys. Rev. B* **2013**, *87*, 201401.
(42) Li, Y. L.; Rao, Y.; Mak, K. F.; You, Y. M.; Wang, S. Y.; Dean, C. R.; Heinz, T. F. *Nano Lett.* **2013**, *13*, 3329−3333.
(43) Kim, C. J.; Brown, L.; Graham, M. W.; Hovden, R.; Havener, R. W.; McEuen, P. L.; Muller, D. A.; Park, J. *Nano Lett.* **2013**, *1*, 5660−5665.
(44) Shen, Y. R. *The Principles of Nonlinear Optics*; Wiley-Interscience: New York, 2003.
(45) van der Veen, M. A.; Vermoortele, F.; De Vos, D. E.; Thierry, V. *Anal. Chem.* **2012**, *84*, 6378−6385.
(46) Hsu, W. T.; Zhao, Z. A.; Li, L. J.; Chen, C. H.; Chiu, M. H.; Chang, P. S.; Chou, Y. C.; Chang, W. H. *ACS Nano* **2014**, *8*, 2951−2958.
(47) Yin, X. B.; Ye, Z. L.; Chenet, D. A.; Ye, Y.; O'Brien, K.; Hone, J. C.; Zhang, X. *Science* **2014**, *344*, 488−490.
(48) Krivanek, O. L.; Chisholm, M. F.; Nicolosi, V.; Pennycook, T. J.; Corbin, G. J.; Dellby, N.; Murfitt, M. F.; Own, C. S.; Szilagyi, Z. S.; Oxley, M. P.; Pantelides, S. T.; Pennycook, S. J. *Nature* **2010**, *464*, 571−574.
(49) Zhou, W.; Zou, X. L.; Najmaei, S.; Liu, Z.; Shi, Y. M.; Kong, J.; Lou, J.; Ajayan, P. M.; Yakobson, B. I.; Idrobo, J. C. *Nano Lett.* **2013**, *13*, 2615−2622.
(50) Lin, Y. C.; Dumcencon, D. O.; Huang, Y. S.; Suenaga, K. *Nat. Nanotechnol.* **2014**, *9*, 391−396.
(51) Wang, L.; Meric, I.; Huang, P. Y.; Gao, Q.; Gao, Y.; Tran, H.; Taniguchi, T.; Watanabe, K.; Campos, L. M.; Muller.; et al. *Science* **2013**, *342*, 614−617.
(52) Zhan, Y. J.; Liu, Z.; Najmaei, S.; Ajayan, P. M.; Lou, J. *Small* **2012**, *8*, 966−971.
(53) Shi, Y.; Zhou, W.; Lu, A.-Y.; Fang, W.; Lee, Y.-H.; Hsu, A. L.; Kim, S. M.; Kim, K. K.; Yang, H. Y.; Li, L.-J.; et al. *Nano Lett.* **2012**, *12*, 2784−2791.
(54) Lee, Y. H.; Zhang, X. Q.; Zhang, W. J.; Chang, M. T.; Lin, C. T.; Chang, K. D.; Yu, Y. C.; Wang, J. T. W.; Chang, C. S.; Li, L. J.; et al. *Adv. Mater.* **2012**, *24*, 2320−2325.
(55) Liu, K.-K.; Zhang, W.; Lee, Y.-H.; Lin, Y.-C.; Chang, M.-T.; Su, C.; Chang, C.-S.; Li, H.; Shi, Y.; Zhang, H.; et al. *Nano Lett.* **2012**, *12*, 1538−1544.
(56) Wu, S. F.; Huang, C. M.; Aivazian, G.; Ross, J. S.; Cobden, D. H.; Xu, X. D. *ACS Nano* **2013**, *7*, 2768−2772.
(57) van der Zande, A. M.; Huang, P. Y.; Chenet, D. A.; Berkelbach, T. C.; You, Y. M.; Lee, G. H.; Heinz, T. F.; Reichman, D. R.; Muller, D. A.; Hone, J. C. *Nat. Mater.* **2013**, *12* (6), 554−561.
(58) Najmaei, S.; Liu, Z.; Zhou, W.; Zou, X. L.; Shi, G.; Lei, S. D.; Yakobson, B. I.; Idrobo, J. C.; Ajayan, P. M.; Lou, J. *Nat. Mater.* **2013**, *12*, 754−759.
(59) Gutierrez, H. R.; Perea-Lopez, N.; Elias, A. L.; Berkdemir, A.; Wang, B.; Lv, R.; Lopez-Urias, F.; Crespi, V. H.; Terrones, H.; Terrones, M. *Nano Lett.* **2013**, *13*, 3447−3454.
(60) Ji, Q. Q.; Zhang, Y. F.; Gao, T.; Zhang, Y.; Ma, D. L.; Liu, M. X.; Chen, Y. B.; Qiao, X. F.; Tan, P. H.; Kan, M.; et al. *Nano Lett.* **2013**, *13*, 3870−3877.
(61) Wang, X. S.; Feng, H. B.; Wu, Y. M.; Jiao, L. Y. *J. Am. Chem. Soc.* **2013**, *135*, 5304−5307.
(62) Lee, Y.-H.; Yu, L.; Wang, H.; Fang, W.; Ling, X.; Shi, Y.; Lin, C.-T.; Huang, J.-K.; Chang, M.-T.; Chang, C.-S.; et al. *Nano Lett.* **2013**, *13*, 1852−1857.
(63) Ling, X.; Lee, Y. H.; Lin, Y. X.; Fang, W. J.; Yu, L. L.; Dresselhaus, M. S.; Kong, J. *Nano Lett.* **2014**, *14*, 464−472.
(64) Gong, Y. J.; Liu, Z.; Lupini, A. R.; Shi, G.; Lin, J. H.; Najmaei, S.; Lin, Z.; Elias, A. L.; Berkdemir, A.; You, G.; et al. *Nano Lett.* **2014**, *14*, 442−449.
(65) Shaw, J. C.; Zhou, H. L.; Chen, Y.; Weiss, N. O.; Liu, Y.; Huang, Y.; Duan, X. F. *Nano Res.* **2014**, *7*, 511−517.
(66) Li, H.; Duan, X.; Wu, X.; Zhuang, X.; Zhou, H.; Zhang, Q.; Zhu, X.; Hu, W.; Ren, P.; Guo, P.; et al. *J. Am. Chem. Soc.* **2014**, *136*, 3756−3759.
(67) Lu, X.; Utama, M. I. B.; Lin, J.; Gong, X.; Zhang, J.; Zhao, Y.; Pantelides, S. T.; Wang, J.; Dong, Z.; Liu, Z.; et al. *Nano Lett.* **2014**, *14*, 2419−2425.
(68) Huang, J.-K.; Pu, J.; Hsu, C.-L.; Chiu, M.-H.; Juang, Z.-Y.; Chang, Y.-H.; Chang, W.-H.; Iwasa, Y.; Takenobu, T.; Li, L.-J. *ACS Nano* **2014**, *8*, 923−930.
(69) Terrones, H.; Del Corro, E.; Feng, S.; Poumirol, J. M.; Rhodes, D.; Smirnov, D.; Pradhan, N. R.; Lin, Z.; Nguyen, M. A. T.; Elias, A. L.; et al. *Sci. Rep.* **2014**, *4*, 4215.
(70) Li, H.; Lu, G.; Wang, Y. L.; Yin, Z. Y.; Cong, C. X.; He, Q. Y.; Wang, L.; Ding, F.; Yu, T.; Zhang, H. *Small* **2013**, *9*, 1974−1981.
(71) Duan, X.; Wang, C.; Shaw, J. C.; Cheng, R.; Chen, Y.; Li, H.; Wu, X.; Tang, Y.; Zhang, Q.; Pan, A.; et al. *Nat. Nanotechnol.* **2014**, *9*, 1024−1130.
(72) Gong, Y.; Lin, J.; Wang, X.; Shi, G.; Lei, S.; Lin, Z.; Zou, X.; Ye, G.; Vajtai, R.; Yakobson, B. I.; et al. *Nat. Mater.* **2014**, *13*, 1135−1142.